Dynamics of Poly(methyl methacrylate) Chains Adsorbed on Aluminum Surfaces

J. Scott Shaffer and Arup K. Chakraborty*

Department of Chemical Engineering, University of California at Berkeley, and Center for Advanced Materials, Lawrence Berkeley Laboratory, Berkeley, California 94720-9989

Received September 8, 1992; Revised Manuscript Received November 16, 1992

ABSTRACT: We present a stochastic model for the dynamics of poly(methyl methacrylate) (PMMA) chains adsorbed on an aluminum surface. The model is able to investigate the relevant length scales and time scales of adsorbed polymers by employing a coarse-grained representation of the polymer chain (in terms of discrete adsorption states) and stochastic dynamics. The dynamics of the adsorbed polymers are governed by a master equation. The transition probabilities that enter the master equation have been derived by applying transition-state theory to the potential energy surface that describes the interactions of the PMMA segments with the aluminum surface. The potential energy surface has been obtained from previous quantum mechanical calculations for oligomers of PMMA near an aluminum surface. By incorporating the details of the segment–surface interactions, we are able to examine the effects of tacticity on the dynamics of adsorbed chains. We find qualitative similarities and quantitative differences between the dynamics of isotactic and syndiotactic PMMA adsorbed on aluminum. The dynamics of PMMA chains share several features with the dynamics of glass-forming liquids. Both systems exhibit nonexponential relaxation and non-Arrhenius temperature dependences of relaxation times. The physical sources of the glasslike dynamical behavior are a rugged energy surface and strong kinetic constraints. The microscopic basis for the kinetic constraints is discussed in detail.

1. Introduction

The study of polymer adsorption at solid surfaces is motivated largely by the widespread technological application of polymer–solid interfaces. Colloidal dispersions, packaging of microelectronics components, composite materials, and biomedical devices are a few examples of applications that depend critically on the integrity of polymer–solid interfaces. Polymer–solid interfaces may be classified into two broad categories based on the nature of the interactions between the polymer segments and the substrate. The first class of interfaces includes those in which the segment–surface interactions are weak and dispersive; the polymers are physisorbed at the interface. The second class of interfaces are those in which the segment–surface interactions are strong and specific; the polymers are chemisorbed at the interface. Polypropylene on graphite is an example of the first class of interfaces; polymer–metal interfaces, such as poly(methyl methacrylate) (PMMA) on aluminum, are examples of the second class. In this work we focus specifically on the PMMA–aluminum system. By analogy, we draw conclusions regarding the behavior of a wide range of strongly interacting polymer–solid interfaces.

Physisorbed polymers at equilibrium are fairly well understood from both theoretical[1-3] and experimental perspectives.[4,5] In contrast, the study of strongly adsorbing polymers has been the subject of only recent attention. Chemisorbing polymers are markedly different from physisorbing polymers for several reasons. First, the segment–surface interactions are much stronger. Second, the chemisorptive interactions are highly specific. The chemisorbing functional groups adsorb preferentially over the more weakly interacting groups. It has been shown recently[6,7] that this preferential adsorption strongly perturbs the rotational conformational statistics from those observed in the bulk or in solution. Third, it has been demonstrated both theoretically[7,8] and experimentally[9] that the adsorbed chains constitute a collection of nonequilibrium structures (a glassy interfacial layer) whose dynamical behavior is similar to that of glass-forming liquids (structural glasses).[10,11] Specifically, relaxation from nonequilibrium states is nonexponential, and the temperature dependence of relaxation times does not follow an Arrhenius law. The trapping of adsorbed polymer chains in nonequilibrium states is a result of the topography of the potential energy surface that characterizes the interactions between the polymer segments and the substrate. Studies of PMMA and aluminum[6] have shown that the potential energy surface is "rugged";[12,13] that is, it contains many local minima and a broad distribution of activation barriers.[14]

The presence of a glassy layer near the polymer–solid interface has several theoretical and practical implications. Of theoretical interest, the dynamics of the polymer chains in the glassy layer are similar to those found in glass-forming liquids.[7-9] These similarities raise interesting questions regarding the underlying physical processes that lead to glassy dynamics. Furthermore, the previous theoretical studies[8] have been performed with simple model polymers. The study of real systems, like PMMA on aluminum, with a rugged energy landscape presents a significant challenge. Overcoming this challenge should lead to insights regarding the microscopic origins of the observed dynamical behavior. From a practical viewpoint, the existence of a glassy interfacial layer implies that the properties of the interface will depend on the history of preparation of the interface. While this has been recognized, the prediction of interfacial properties as a function of history for specific systems remains an outstanding long-term goal.

On the basis of the discussion above, it should be clear that strongly interacting polymer–solid interfaces have many special features whose theoretical analysis requires different methods than those used to study weakly physisorbed polymers. The interaction potentials cannot be constructed from simple, pairwise additive potentials. Since the interactions are chemical in nature, interaction potentials must be derived from electronic structure calculations.[6,15] Once the interactions have been well

* Author to whom correspondence should be addressed.

0024-9297/93/2226-1120$04.00/0

characterized, the equilibrium statistics of interfacial chains could be generated by the techniques that have been applied to weakly interacting systems.[1,2] It has been argued, however, that the interfacial chains are not in equilibrium but rather are constrained in nonequilibrium states.[7] Therefore, the study of these systems must address not only static features but also the dynamics of adsorption. Furthermore, the dynamics must be sampled from a wide range of initial conditions. In that way, the history dependence of the interfacial structures can be addressed, and the appropriate nonequilibrium averages can be calculated. The final concern is the presence of very long time scales. Since the interactions of the polymer segments with the surface are so strong, the effective activation energy for conformational transitions or local desorption of segments is much larger than the thermal energy, k_BT, at room temperature and below. The corresponding relaxation times can range from milliseconds to hours, and even beyond experimental time scales. Thus the important adsorption events occur over time scales that are impossible to probe using traditional molecular dynamics simulations; an alternative simulation procedure must be developed.

The goal of this work is to develop a stochastic model of the dynamics of PMMA adsorption on an aluminum surface that can achieve the necessary goals for the study of strongly interacting interfaces set forth above. The stochastic model incorporates the details of the strength and specificity of the interaction potential; it follows the dynamics of the adsorption process explicitly; and it has the computational efficiency to probe the experimentally relevant time scales and average over many different initial conditions. By incorporating the details of the interaction potential, the model can also investigate the effect of the tacticity of PMMA on the dynamics of adsorption. The model is currently limited to isolated polymer chains, so it is most directly applicable to adsorption from dilute solutions. Nevertheless, we expect the physical phenomena revealed by the model to be important for interacting chains and for adsorption from concentrated solutions. This point will be addressed in more detail later.

The format of the paper is as follows. In section 2 we review the relevant features of the PMMA–aluminum system and formulate the stochastic model for the dynamics of strongly adsorbed polymer chains. In section 3 we describe the potential energy function used to model the interactions of PMMA with aluminum. The computational methods used in the study are given in section 4. In section 5 the results of the stochastic simulations of adsorbed chains are presented and discussed. The results are interpreted in view of theories developed for other glassy materials and compared with recent experimental work on polymer adsorption. Concluding remarks are offered in section 6.

2. Model Development and Theory

2.1. Overview. Our goal is to construct a model for the dynamics of PMMA chains adsorbed on aluminum surfaces. First we review the important features of the PMMA–aluminum interface. The interactions between segments of PMMA and an aluminum surface are strong and specific. In particular, the interaction energy between PMMA segments and an aluminum surface is highly dependent on the orientation and configuration in which segments approach the surface.[6] The orientation dependence arises because the methacrylate side group of PMMA contains a carbonyl group and an ester oxygen atom that may chemisorb at the surface, while the alkyl backbone of the polymer cannot interact so strongly. Binding energies for chemisorption of the carbonyl group range from approximately 50 to 100 kJ mol^{-1}, while the interaction of the ester oxygen atom is weaker, with binding energies ranging from approximately 20 to 50 kJ mol^{-1}. In orientations in which either chemisorbing functional group can approach the surface, there is an activation energy to adsorption of approximately 50 kJ mol^{-1}. Activation energies for the complete desorption of segments range from 100 to 150 kJ mol^{-1}, while activation energies for conformational transitions between different chemisorbed conformations are much lower, approximately 50 kJ mol^{-1}.

By considering the strength of the interactions, we see immediately that conventional molecular dynamics (MD) simulations cannot probe the time scales relevant to the PMMA–aluminum system. For example, from the activation energies listed above, we can estimate that the time scale for conformational relaxation of adsorbed segments at 300 K will be on the order of 10^{-3} s. Furthermore, the existence of a glassy interfacial layer[7] requires the calculation of nonequilibrium averages over the initial configuration space. As a result, simulations must explore many different realizations of the adsorption process subject to a wide range of initial conditions. Given that a single MD simulation of polymer and solvent can realistically probe only 10^{-8} s, it is clear that the application of MD simulations to this problem is an impossible task.

Recently, Chakraborty and Adriani have proposed a kinetic Ising model[8,16,17] to address the shortcomings of MD simulations. The model does not address PMMA–aluminum interfaces specifically but rather considers a generic representation of a strongly adsorbing polymer which contains two functional groups per segment ("stickers") that can bind strongly to a surface. This polymer architecture is a schematic representation of PMMA, in which both the carbonyl group and ester oxygen atom may chemisorb on aluminum.[6] We note that other simple chain architectures have been considered in ref 8. The fundamental premise of the kinetic Ising model is that once the polymer is adsorbed in an initial nonequilibrium conformation, the only relevant information is whether each sticker is adsorbed or desorbed. In other words, the explicit atomic degrees of freedom of the polymer and solvent are discarded, and each sticker is mapped onto a two-state system, or an Ising spin variable. The spin variables then evolve in time according to dynamical rules that were chosen based on physical considerations that reflect the polymer chain connectivity. The dynamical rules account for local torsional strain, steric hindrance, and entropic constraints imposed by the surface. By using such a description, the model revealed that the dynamics of strongly adsorbed polymer chains were akin to those of glass-forming liquids. For example, the simulations reveal that the interfacial chains are locked into nonequilibrium conformations at low temperatures. At intermediate temperatures, the chains can relax to equilibrium in reasonable times, but the dynamics are very sluggish, showing similarities to bulk glass-forming liquids. In particular, the relaxation to equilibrium was found to be nonexponential; the dynamics could be described with a stretched-exponential, or Kohlrausch–Williams–Watts (KWW), function:

$$q(t) = \exp[-(t/\tau_{KWW})^{\beta}] \quad (1)$$

where $q(t)$ is a nondimensional measure of relaxation to equilibrium, and β and τ_{KWW} are adjustable parameters. Also, the temperature dependence of the relaxation times, τ, did not follow an Arrhenius law but showed a divergence

that was described by the Vogel–Fulcher equation:

$$\tau(T) = \tau_{VF} \exp\left[\frac{E_{VF}}{k_B(T - T_{VF})}\right] \quad (2)$$

The parameter T_{VF} physically corresponds to a temperature at which the relaxation time diverges or exceeds observational time scales due to dynamical falling out of equilibrium. The Vogel–Fulcher equation, which predicts a diverging relaxation time, should be contrasted with the Arrhenius form

$$\tau(T) = \tau_0 \exp(E_{Arr}/k_B T) \quad (3)$$

which predicts a finite relaxation time for any finite temperature. In eq 3, E_{Arr} is an effective activation energy and τ_0 is an intrinsic microscopic relaxation time.

To examine the adsorption of PMMA on aluminum, we take an approach similar to the kinetic Ising models of adsorbed chain dynamics proposed in ref 8: we adopt a "coarse-grained" stochastic model, one that follows the dynamics of a reduced set of degrees of freedom. The details of the model and the simulation technique, however, are quite different from ref 8 because we incorporate the features of the segment–surface interactions that are specific to the PMMA–aluminum interface. The formulation to be developed in this paper has three important components: (1) Each monomer of the polymer chain is classified into one of four discrete states based on the sorption state of the two chemisorbing functional groups. Information regarding the sorption states is obtained from an analysis of the PMMA–aluminum potential energy surface obtained from quantum mechanical calculations.[6] (2) The time evolution of the polymer configuration is modeled as a stochastic process governed by a master equation. The transition probabilities that enter the master equation play a crucial role in determining the dynamical behavior. In simple treatments,[8] phenomenological rules were invented to construct a model for the transition probabilities. In our model, the transition probabilities are obtained from the application of transition-state theory to the detailed potential energy surface that characterizes the PMMA–aluminum system. (3) Particular realizations of the adsorption dynamics are obtained by numerical solution of the governing master equation. We will now describe each part of the formulation in turn.

2.2. Discrete-State Classification. It is known from MD simulations[7,8] and experiments[18] that the first step of adsorption from solution is fast. It is the subsequent relaxation of the adsorbed chains from this initial nonequilibrium state that is of interest here. Once the PMMA chain is in a nonequilibrium conformation with a few segments adsorbed, the important events during the relaxation to equilibrium will be the adsorption and desorption of the chemisorbing functional groups, the carbonyl group and the ester oxygen.[6] It is appropriate, then, to take a coarse-grained representation of the polymer chain in which an integer label, Q, is associated with each monomer of the chain according to the sorption state of the carbonyl group and the ester oxygen atom. Specifically, each monomer can be present in one of four discrete states: (1) the carbonyl group adsorbed, ester oxygen desorbed; (2) carbonyl group desorbed, ester oxygen adsorbed; (3) both functional groups adsorbed; and (4) both functional groups desorbed. (Polymer segments with both functional groups adsorbed will frequently be referred to as "strongly adsorbed"; segments with both functional groups desorbed will often be called "free" segments.) A particular functional group is considered to be adsorbed if it resides closer than 4 Å to the surface; this choice is based on the location of the attractive part of the potential energy surface obtained in ref 6. It is important to note that each discrete state is comprised of *many* stable conformations (local minima on the potential energy surface) that differ only in degrees of freedom that are irrelevant for the chemisorption of segments. The torsion angle of a weakly interacting pendant methyl group is an example of an irrelevant degree of freedom.

2.3. Transition Probabilities. Given the coarse-grained description of the polymer configuration, the heart of the stochastic model is the specification of the rate constants, or transition probabilities, for transitions between the various discrete states. As noted above, in the kinetic Ising model of ref 8 the transition rates were postulated based on physical considerations of the polymer chain connectivity. Here, however, we will calculate rate constants directly from the potential energy surface by applying transition-state theory. With the discrete-state classification given above, the configuration of an adsorbed polymer chain of N segments is given by the set of N integers $\{Q_1, Q_2, ..., Q_N\} \equiv \mathbf{Q}$. The configuration space of the adsorbed polymer is reduced to the 4^N possible arrangements of the monomer state variables. The fundamental quantities that we seek are the rate constants $R(\mathbf{Q}\rightarrow\mathbf{Q}')$, the transition probabilities per unit time for the polymer chain to undergo a change from configuration $\mathbf{Q}$ to configuration $\mathbf{Q}'$. Once these transition probabilities are specified, the statistical behavior of the adsorption process is completely determined by the master equation[19]

$$\frac{dP(\mathbf{Q},t)}{dt} = \sum_{\mathbf{Q}'} [R(\mathbf{Q}'\rightarrow\mathbf{Q})\, P(\mathbf{Q}',t) - R(\mathbf{Q}\rightarrow\mathbf{Q}')\, P(\mathbf{Q},t)] \quad (4)$$

where $P(\mathbf{Q},t)$ is the probability of the polymer chain being in configuration $\mathbf{Q}$ at time t.

We make the assumption that only one monomer at a time changes its sorption state. The transition probabilities above can then be written $R(Q_i\rightarrow Q'_i|\mathbf{Q})$, the probability per unit time for monomer i to make a transition from state Q_i to state Q'_i, given that the polymer chain is in configuration $\mathbf{Q}$. The rate constants for any given monomer to change its sorption state depend on the current state of the monomer because the segment–surface potential is orientation and configuration dependent. The rate constants also depend on the states of neighboring monomers because of torsional strain and steric hindrance; this is a local effect mediated through the torsional and nonbonded interaction potentials. There is also a nonlocal effect on the rate constants from the configurational entropy change that accompanies the adsorption or desorption of polymer segments. To account for these separate effects, we factor the rate constant into local and nonlocal terms as follows:

$$R(Q_i\rightarrow Q'_i|\mathbf{Q}) = R_L(Q_i\rightarrow Q'_i|Q_{i-1},Q_{i+1})\, R_{NL}(Q_i\rightarrow Q'_i|\mathbf{Q}) \quad (5)$$

The factorization above is appealing because it separates the configurational entropy, which is generic to all polymer–solid interfaces, from the local effects that are unique to each polymer–solid system considered. We further assume that the local effects on the adsorption and desorption rates of a given monomer can be represented by accounting for the instantaneous states of its two nearest neighbors only. As a result, the quantities $R_L(Q_i\rightarrow Q'_i|Q_{i-1},Q_{i+1})$ can be derived from the potential energy surface of a trimer of PMMA interacting with an aluminum surface. Note that the effect of the tacticity of the PMMA chains is incorporated explicitly in this

treatment. For the isotactic chain, the transition probabilities are calculated using a PMMA trimer consisting of two meso diads; for the syndiotactic chain, they are calculated using a trimer consisting of two racemic diads. The calculation of the nonlocal rate factors $R_{NL}(Q_i \rightarrow Q'_i|\mathbf{Q})$ requires the treatment of the configurational entropy of polymer chains near surfaces. Below we describe our treatment of both contributions to the transition probabilities.

Discrete-State Transition-State Theory. As noted earlier, we make the assumption that the local effects on the transition rates of a PMMA monomer can be captured by considering only the instantaneous states of its nearest neighbors. Since only three monomers are involved, we can determine all local rate constants, $R_L(Q_i \rightarrow Q'_i|Q_{i-1},Q_{i+1})$, by applying transition-state theory (TST) to the potential energy surface of a PMMA trimer interacting with aluminum. In traditional applications of TST, the configuration space is divided into regions, called "microstates", that contain a single local minimum on the potential energy surface.[20,21] The microstates are separated by dividing surfaces that contain transition states, first-order saddle points on the potential energy surface. Using one of several theoretical prescriptions,[22] a first-order rate constant can be calculated for transitions between microstates. Here, however, within the coarse-grained classification of polymer configurations into discrete sorption states, each discrete state will encompass *many* microstates. Furthermore, there will be many conformational transitions within a discrete state, as well as many possible transition paths between discrete states. Given a complete catalog of potential energy minima, transition states, and the rate constants for jumps between minima, a method is required to construct the overall transition probabilities, R_L, between the discrete states by appropriately weighting the individual rate constants.

The construction of the overall rate constants involves an argument based on the separation of time scales between conformational transitions of unreactive side groups and the activated adsorption and desorption of chemisorbing functional groups. Consider a large number of microstates that have been classified into one of two "macrostates", based on a clear physical distinction. For example, for a PMMA trimer near an aluminum surface, the first macrostate may contain all locally stable conformations in which only the carbonyl group of the middle segment is chemisorbed to the surface; the second macrostate may contain all stable conformations in which only the ester oxygen atom of the middle segment is chemisorbed to the surface. Suppose now that all reaction paths for transitions between the individual potential energy minima (microstates) are known. The reaction paths can be distinguished as to whether or not they cross a macrostate boundary, that is, whether the microstates involved (the initial and final points in configuration space) belong to the same macrostate or to two different macrostates. Reaction paths that connect two microstates within the same macrostate will generally correspond to a simple conformational transition of a weakly interacting side group. For such transitions, the activation energies are relatively low. Conversely, paths that connect two microstates in different macrostates will involve the desorption of a chemisorbed functional group or the adsorption of a different group. The corresponding activation barriers are very high compared to the activation energies of simple conformational transitions. As a result, the rate constants for transitions between two microstates *within* the same macrostate will be orders of magnitude higher than rate constants for transitions *between* macrostates. The discrepancy in the rate constants leads to a separation of time scales between the two classes of events.

Given the separation of time scales as outlined above, it is a good approximation to treat the microstates within a given macrostate as locally equilibrated during the time intervals between jumps from one macrostate to another. In other words, once the system makes a transition from one macrostate to another, the microstates within the final macrostate quickly become populated with the probability distribution

$$p_i^A = Z_A^{-1} \int_i \exp[-V(\mathbf{x})/k_B T]\, d\mathbf{x} \tag{6}$$

In the equation above, p_i^A is the probability of microstate i in macrostate A being occupied when the system is restricted to macrostate A, $\mathbf{x}$ represents the configurational degrees of freedom (atomic Cartesian coordinates), $V(\mathbf{x})$ is the potential energy function, and the integration is limited to the region of configuration space belonging to microstate i. The normalization factor Z_A is the *local* configurational partition function for macrostate A:

$$Z_A = \int_A \exp[-V(\mathbf{x})/k_B T]\, d\mathbf{x} \tag{7}$$

where the integration for Z_A is over the configuration space of all microstates that have been grouped into macrostate A.[23] Clearly eq 6 applies only on time scales shorter than the average time required to make transitions to other macrostates. Since the microstate populations are rapidly redistributed before the system has a chance to jump to another macrostate, the individual rate constants for transitions out of the macrostate must be weighted according to eq 6. The effective rate constant for transitions between macrostate A and another macrostate B is then calculated by

$$R_{A \rightarrow B} = \sum_{i \leftrightarrow j} p_i^A k_{i \rightarrow j} \tag{8}$$

where $R_{A \rightarrow B}$ is the overall effective rate constant (transition probability per unit time) for transitions from macrostate A to macrostate B. The sum is over all individual reaction paths that connect microstates in macrostate A with microstates in macrostate B; the $k_{i \rightarrow j}$ represent the rate constants for the individual transitions between microstates. By summing over all paths between the macrostates, the effective rate constants account for entropic bottlenecks in configuration space in addition to potential energy barriers for individual reaction paths. In effect, the potential energy surface of the full configuration space has been mapped onto a *free energy* surface of much lower dimensionality.[23] In the Appendix it is shown that the effective rate constants defined by eq 8 satisfy the condition of detailed balance for the macrostate populations.

Configurational Entropy. The entropic constraints associated with changing the loop, train, and tail distributions by adsorption or desorption are represented through the rate constant $R_{NL}(Q_i \rightarrow Q'_i|\mathbf{Q})$ in eq 5. In general, R_{NL} can depend on the entire configuration of the polymer chain, as well as the current and target states of the specified segment. The change in entropy for a given event can be estimated by counting the number of configurations, W, available in loops and tails, and using the formula $S = k_B \ln W$. The following expressions can be derived for random walks on lattices confined to one side of a surface plane:[4,24,25]

$$W_L(n) = (2\pi)^{-1/2} 2^n n^{-3/2} \quad (9)$$

$$W_T(n) = (2\pi)^{-1/2} 2^n n^{-1/2} \quad (10)$$

where W_L and W_T are the number of conformations available to a loop and tail, respectively, comprised of $n - 1$ segments. By using expressions for random walks in one dimension, we implicitly account for the fact that, in the random-walk model, the interface does not affect the configurational freedom in the two coordinate directions parallel to it. The factors $n^{-3/2}$ and $n^{-1/2}$ in eqs 9 and 10 indicate the loss of configurational entropy associated with forming loops and tails. They also show that one long loop is entropically favored over two shorter loops.

For transitions between different adsorbed states of the same segment, R_{NL} is obviously unity. For transitions that involve adsorption or desorption, we must work out transition rates for adsorption–desorption events that satisfy detailed balance. The ratio of rate constants must be equal to $\exp(\Delta S/k_B)$, where ΔS is the entropy change that accompanies the event. We choose $R_{NL} = \exp(\Delta S/k_B)$ for adsorption events and $R_{NL} = 1$ for the corresponding desorption events. Thus the rate constant for adsorbing a loop or tail segment is lowered due to the negative entropy change.

2.4. Time Evolution. To study the dynamics of polymer adsorption, we must obtain solutions to the governing master equation, eq 4, for the time evolution of the probability $P(\mathbf{Q},t)$ of each possible configuration. The high dimensionality of the problem and the long-range correlations introduced by the entropic constraints preclude an analytical solution. Instead, we perform stochastic simulations of the adsorption process starting from many different initial conditions and accumulate averages. The stochastic simulations employ the theory of pure Markov jump processes.[26,27] To use this theory, we assume that, for each configuration of the polymer chain, all possible adsorption and desorption events (the "elementary events") are independent Poisson processes. That is, each possible event $Q_i \rightarrow Q'_i$ has a first-order rate constant $R = R(Q_i \rightarrow Q'_i|\mathbf{Q})$ associated with it, as discussed above. The time interval between events is an exponentially distributed random variable:

$$F(t) = R \exp(-Rt) \quad (11)$$

where $F(t)$ is the probability density for the distribution of time intervals between events. The average time between events, $\langle t \rangle$, is calculated as

$$\langle t \rangle = \int_0^\infty t\, F(t)\, dt \quad (12)$$

and is equal to the inverse of the rate constant, $1/R$.

Several properties of exponentially distributed random variables[28] have been used to construct the simulation algorithm. Consider n distinct stochastic events governed by Poisson statistics according to eq 11, with rate constants $R_1, R_2, ..., R_n$, that occur in time intervals $t_1, t_2, ..., t_n$. The time interval for the first event to occur, $\tau_1 = \min(t_1, t_2, ..., t_n)$, is also an exponentially distributed random variable with an overall rate constant, ρ, equal to the sum of all the individual rate constants:

$$\rho = \sum_{i=1}^{n} R_i \quad (13)$$

The probability that the ith event will occur first is given by

$$P_i = R_i/\rho \quad (14)$$

so that the total probability is normalized. It can also be shown that the stochastic process consisting of the n events is Markovian.[26]

Using the properties of the Markov jump process defined above, the implementation of the simulation algorithm is straightforward.[21] The initial configuration of the adsorbed polymer is generated randomly. The rate constants (transition probabilities) for each possible adsorption and desorption event are calculated based on the current chain configuration, as outlined above. The rate constants are then summed according to eq 13, and the time interval τ_1 to the first event is sampled from the probability distribution of eq 11 with rate constant ρ. The time τ_1 is then added to the simulation clock. Finally, the actual event to occur at this time step is chosen from the probability distribution of eq 14. Once the time and event have been determined stochastically, the polymer configuration is updated and a new step in the simulation begins.

This simulation procedure, in which the time step as well as the sorption events are stochastic variables, has the great advantage that one event occurs at each step in the simulation. We never have to *wait* for an event to occur, but rather the time step os the simulation adjusts to the underlying time scale of the physical process. This feature is especially valuable in simulating the dynamics of strongly adsorbed polymers. The first phase of the adsorption process is very fast,[8,18] but the ultimate relaxation to equilibrium can be extremely slow, and even surpass experimental time scales. Thus, the adaptive time step is essential in following the relaxation to equilibrium at low temperatures.

3. Potential Energy Function

To have a realistic model of adsorbed chain dynamics at PMMA–aluminum interfaces, the transition probabilities in the stochastic model must incorporate the physics and chemistry of the PMMA–aluminum system. As discussed in section 2, the quantities $R_L(Q_i \rightarrow Q'_i|Q_{i-1},Q_{i+1})$ can be derived from the potential energy surface of a trimer of PMMA interacting with an aluminum surface. In this section, we present the potential energy function that models the intramolecular potential for a PMMA trimer and the potential that describes the interactions of a PMMA trimer with an aluminum surface.

The potential energy function, V, for the PMMA–aluminum system is the sum of the intramolecular potential, V^{intra}, for the PMMA trimer alone, and the surface potential, V^{surf}, that describes the interaction of the PMMA trimer with the aluminum surface. The intramolecular potential has been adapted from previous work of Vacatello and Flory.[29] For computational efficiency, all pendant methyl groups ($-CH_3$) and backbone methylene groups ($-CH_2-$) are treated as united atoms. Furthermore, all bond lengths and bond angles are fixed. Following ref 29, the intradiad bond angle (denoted by τ' in ref 29) is fixed at 124°; the interdiad bond angle (denoted by τ in ref 29) is fixed at 111°. All other bond angles and all bond lengths are fixed at their minimum energy values. With the simplification of constant bond lengths and bond angles, the intramolecular potential is written as follows:

$$V^{intra} = \sum_{\phi_i} V_i^{tor}(\phi_i) + \sum_{i<j} \left[\frac{A_{ij}}{r_{ij}^{12}} - \frac{B_{ij}}{r_{ij}^{6}} + \frac{q_i q_j}{\epsilon r_{ij}} \right] \quad (15)$$

The first term is a sum over all torsion angles ϕ_i; V_i^{tor} is

Table I
Atomic Data for Calculating Lennard-Jones Parameters from the Slater–Kirkwood Formula

atom	van der Waals radius, Å	effective no. of electrons	polarizability, Å^3
C	1.8	5	0.93
C (carbonyl)	1.8	5	1.23
O (carbonyl)	1.6	7	0.84
O (ester)	1.6	7	0.70
CH_2 or CH_3[a]	2.0	7	1.77

[a] Sundararajan, P. R.; Flory, P. J. *J. Am. Chem. Soc.* 1974, *96*, 5025.

Table II
Lennard-Jones Parameters between "Nonbinding" Atoms in PMMA and Aluminum for Use in eqs 16 and 17

atom	ϵ_i, kJ mol^{-1}	σ_i, Å
C	7.29	2.88
C (carbonyl)	9.13	2.88
CH_2 or CH_3	5.37	3.24

the potential specific for each distinct torsion angle given in ref 29. The second term is a sum over all nonbonded pairs. The distance between atoms i and j is denoted by r_{ij}; partial charges are denoted by q_i and q_j. Lennard-Jones potentials, with parameters A_{ij} and B_{ij}, act between all nonbonded pairs; the Coulomb potential, represented by the last term, acts only between the atoms in the methacrylate side groups that carry significant partial charges. The parameters for the torsional potentials, partial charges, and the dielectric constant, ϵ, are taken directly from ref 29. The Lennard-Jones parameters B_{ij} are calculated from the Slater–Kirkwood formula, with the atomic parameters given in Table I; the set of A_{ij} are calculated such that the Lennard-Jones potential between groups i and j is a minimum at the sum of their van der Waals radii.

The surface potential, V^{surf}, has been derived from a previous quantum mechanical study[6] of PMMA oligomers near an aluminum surface in which the carbonyl bond was allowed to relax upon chemisorption. An empirical force field was presented in ref 6; here, however, we have taken the same interaction energies as those of ref 6 and fit them to a slightly different functional form. For the purpose of the interaction potential, the atoms in PMMA are divided into two groups: the two oxygen atoms of each PMMA monomer are considered to be "binding"; all other atoms are "nonbinding". The nonbinding atoms interact with the surface through a purely repulsive, truncated and shifted Lennard-Jones potential:[30]

$$V_i^{non} = \frac{2}{3}\pi\sigma_i^3\epsilon_i\rho_{Al}\left[\frac{2}{15}\left(\frac{\sigma_i}{z_i}\right)^9 - \left(\frac{\sigma_i}{z_i}\right)^3 + \frac{2}{3}\left(\frac{5}{2}\right)^{1/2}\right] \quad \text{for} \quad z_i \le \left(\frac{2}{5}\right)^{1/6}\sigma_i \quad (16)$$

$$V_i^{non} = 0 \quad \text{for} \quad z_i > \left(\frac{2}{5}\right)^{1/6}\sigma_i \quad (17)$$

In the equations above, V_i^{non} is the potential for nonbinding atom i; z_i is the distance of atom i from the aluminum surface; ρ_{Al} is the number density of aluminum atoms, 0.0603 Å^{-3}; σ_i and ϵ_i are Lennard-Jones parameters between the nonbinding atoms of PMMA and the aluminum atoms in the substrate. The Lennard-Jones parameters for use in eqs 16 and 17 are given in Table II. In calculating the parameters from the Slater–Kirkwood formula, the polarizability of aluminum was taken from the work of de Heer et al.[31] on large aluminum clusters.

Table III
Coefficients for the "Binding" Potentials (Equations 18–20)

Shared Parameters	
A = 50.0 kJ mol^{-1}	z_b = 2.0 Å
λ = 1.1 Å^{-1}	
Ester Oxygen Parameters, kJ mol^{-1}	
B = 157.0	C = 87.0
Carbonyl Oxygen Parameters, kJ mol^{-1}	
β_0 = 148.7	γ_0 = 114.3
β_1 = 47.4	γ_1 = −28.4
β_2 = −4.9	γ_2 = −49.9

The chemisorption of PMMA to aluminum is described by using a modified Morse potential for the binding atoms:

$$V_i^{bind} = A_i \exp[-2\lambda(z_i - z_b)] - B_i \exp[-\lambda(z_i - z_b)] + C_i\lambda^2(z_i - z_b)^2 \exp[-\lambda(z_i - z_b)] \quad (18)$$

where V_i^{bind} is the potential for binding atom i. The first two terms of eq 18 form the standard Morse potential; the third term represents the activation energy for chemisorption. The values of A, λ, and z_b in Table III; they are the same for both the carbonyl and ester oxygen atoms. Table III also contains the values of the coefficients B and C for the ester oxygen atom. The orientation dependence of the binding and activation energies is incorporated in the coefficients B and C for the carbonyl oxygen atom. The coefficients are not constant but depend on the orientation of the carbonyl group as follows:

$$B = \beta_0 + \beta_1 \cos\theta + \beta_2 \cos^2\theta \quad (19)$$

$$C = \gamma_0 + \gamma_1 \cos\theta + \gamma_2 \cos^2\theta \quad (20)$$

where θ is the angle between the surface normal vector and the vector drawn from the carbonyl oxygen atom to the carbonyl atom. (The angle $\theta = 0$ if the carbonyl group is perpendicular to the surface, with the carbonyl oxygen atom closer to the surface than the carbonyl carbon atom.) Table III contains the values of the constants used in eqs 19 and 20. The parameters in eqs 18–20 were fit to the results of the quantum mechanical calculations reported in ref 6. (Prior to the fitting procedure, the parameters in eqs 16 and 17 were fixed according to the values in Table II and were not adjusted.) Finally, the total interaction potential between the PMMA trimer and the aluminum surface, V^{surf}, is simply the sum of the individual contributions from each V_i^{non} and V_i^{bind}.

4. Computational Methods

A prerequisite for the application of TST is the location of all relevant extrema (minima and first-order saddle points) and the associated reaction paths on the potential energy surface.[32] We accomplish this task in two steps. First, we perform a conformational search that locates the saddle points on the potential energy surface. Then, we trace the reaction paths from transition states to potential energy minima by following steepest-descent paths.

The conformational search for saddle points is based on the "usage-directed" searching algorithm described in detail by Chang et al.[33] for the location of potential energy minima in organic molecules. The only modification in our procedure is to search for first-order saddle points instead of minima. Starting from a given point on the potential energy surface (generated according to the algorithm given in ref 33), we use the rational function optimization (RFO) method[34,35] to step along the potential energy surface to the "nearest" first-order saddle point. This transition state is then compared to the existing

database of previously located transition states. The iterative search procedure is continued until no new transition states are located in 10 000 attempts. The RFO method requires that the Hessian matrix of second derivatives of energy with respect to coordinates be evaluated and diagonalized. This is computationally demanding but still feasible, with the number of degrees of freedom in the PMMA trimer.

After the transition states have been located and cataloged, the reaction paths and potential energy minima are obtained by following steepest-descent paths in mass-weighted coordinates from the transition states down to the associated minima. The steepest-descent paths are initiated along the single direction of negative curvature at the transition state as indicated by the Hessian eigenvector associated with the single negative eigenvalue. The first steepest-descent path originates parallel to this eigenvector; the second originates antiparallel to this eigenvector. The potential energy minima that are connected by a reaction path that goes through the transition state are then identified as the terminal points of the two steepest-descent paths.

The calculation of the transition probabilities $R_L(Q_i \rightarrow Q'_i|Q_{i-1},Q_{i+1})$ calls for the evaluation of the configurational integrals defined in eqs 6 and 7. In principle, Monte Carlo techniques could be used, but the high dimensionality of the potential energy surface and the number of minima (greater than 30 000) make the computation unfeasible. For simplicity, the local equilibrium probabilities p_i^A were calculated as

$$p_i^A = Z_A^{-1} \exp(-V_i/k_B T) \tag{21}$$

where V_i is the potential energy at the minimum that defines microstate i. The local partition function, Z_A, is given by

$$Z_A = \sum_{j \in A} \exp(-V_j/k_B T) \tag{22}$$

where the sum is taken only over microstates in macrostate A. Given a pair of potential energy minima and the transition state that connects them, the first-order rate constants were calculated simply as

$$k_{i \rightarrow j} = k_0 \exp[-(V_{TS} - V_i)/k_B T] \tag{23}$$

$$k_{j \rightarrow i} = k_0 \exp[-(V_{TS} - V_j)/k_B T] \tag{24}$$

where $k_{i \rightarrow j}$ is the rate constant for transitions from minimum (microstate) i to minimum j, and vice versa; V_{TS} is the potential energy of the transition state; V_i and V_j are the potential energies of the minima. The prefactor k_0 was chosen to be 10^{12} s^{-1} to reflect the order of magnitude of the attempt or collision frequency for activated processes in solution.[36] The rate constants could have been calculated more accurately by applying TST for multidimensional, multistate systems and accounting for dynamical corrections,[37,38] but the number of distinct reaction paths (on the order of 10^5) prohibited the more detailed calculations. By using only the potential energy at the minimum in eqs 21 and 22, we are implicitly assuming that the entropic contribution to the equilibrium probabilities is comparable for all stable conformations. Similarly, by using a constant prefactor in eqs 23 and 24, we assume that the configurational entropies of the transition states are comparable to those of the stable states.

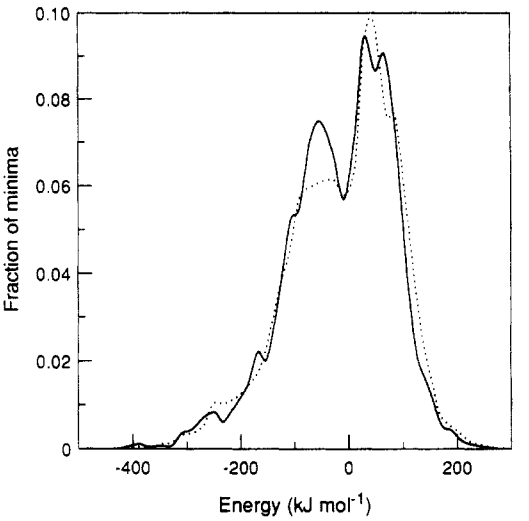

Figure 1. Distribution of potential energy minima for a PMMA trimer interacting with an aluminum surface. The solid line corresponds to the meso–meso trimer (model compound for isotactic PMMA chains); the dotted line corresponds to the racemic–racemic trimer (model compound for syndiotactic PMMA chains).

5. Results and Discussion

5.1. Energy Distributions. Before proceeding to the discussion of the dynamics of PMMA chains adsorbed on aluminum, we discuss two features of the PMMA–aluminum potential energy surface: the distribution of potential energy minima and the distribution of activation barriers to conformational transitions and adsorption–desorption events. These energy distributions illustrate the structure of the potential energy surface at the "local" level of PMMA trimers. The potential energy surface at this level determines the transition probabilities $R_L(Q_i \rightarrow Q'_i|Q_{i-1},Q_{i+1})$. The conformational searches for reaction paths for the isotactic and syndiotactic trimers of PMMA near an aluminum surface discovered more than 30 000 minima and 100 000 transition states for each stereoisomer. There are still more extrema that were not cataloged because of limitations in computational resources. The main source of difficulty is that the efficiency of the conformational search, defined as the probability of finding a new saddle point on a given trial, decreases rapidly as the number of trials increases. Nevertheless, the large database of extrema should provide a good statistical description of the full set of minima and transition states. Furthermore, because individual transitions are weighted by their probability of occurrence according to eq 8, only a statistical sampling of the potential energy surface is required to construct the coarse-grained rate constants.

The distributions of potential energy minima for the isotactic and syndiotactic trimers are presented in Figure 1. The figure shows the fraction of minima as a function of the potential energy of the combined PMMA trimer–aluminum system. The zero of energy in each case corresponds to the most stable conformation of the PMMA trimer in vacuum. Note that the distribution of energy minima is very broad, both for adsorbed ($V_i < 0$) and desorbed ($V_i \geq 0$) trimers. The minima with the lowest energies ($V_i \approx -400$ kJ mol^{-1}) are those in which all three monomers have chemisorbed to the surface with both the carbonyl group and ester oxygen atom. Only a small fraction (0.005) of the conformations, however, allow strong chemisorption to the aluminum surface; most conformations in which all three monomers chemisorb have higher energies. In these configurations, a high degree of torsional

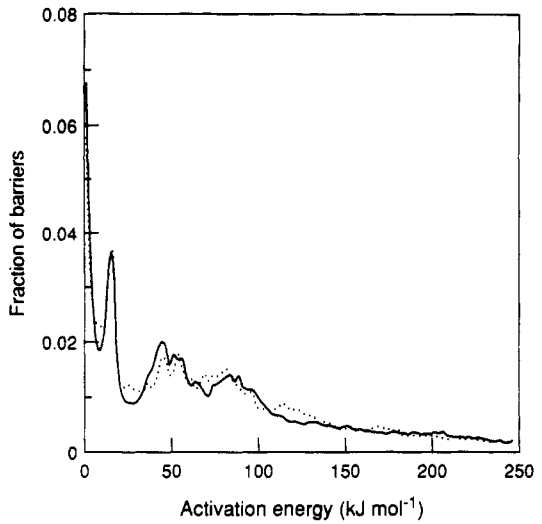

Figure 2. Distribution of activation energies for conformational and adsorption–desorption transitions of a PMMA trimer interacting with an aluminum surface. The solid line corresponds to the meso–meso trimer (model compound for isotactic PMMA chains); the dotted line corresponds to the racemic–racemic trimer (model compound for syndiotactic PMMA chains).

strain or steric crowding occurs to accommodate the chemisorption. As a result of the wide energy distribution, the effective free energy of adsorption per monomer and the adsorbed chain conformations will be temperature dependent. The strongly bound configurations will dominate at low temperatures, while the more weakly bound configurations will become populated at higher temperatures.

Figure 2 shows the distributions of activation barriers for transitions between potential energy minima of the PMMA–aluminum system. These events include conformational transitions between different adsorbed configurations and transitions between adsorbed and desorbed configurations. The distributions for the two trimer tacticities are very similar. The large fraction of events with activation energies close to zero are transitions between very similar adsorbed configurations. The sharp peak in the distributions for both stereoisomers between 15 and 20 kJ mol^{-1} corresponds to conformational transitions of backbone and pendant group torsion angles in desorbed monomers. The fairly wide clusters of activation energies centered around 50 and 80 kJ mol^{-1} are barriers for conformational rearrangement of chemisorbed segments and for the activated adsorption of segments. Finally, the long tail of barriers at higher activation energies correspond to transitions with a greater degree of steric hindrance than the lower energy transitions. Note that the distributions in Figure 2 are similar, but not identical, for the two stereoisomers. The effects of these wide energy distributions (both for minima and for activation barriers) on the dynamical properties of adsorbed isotactic and syndiotactic PMMA chains are discussed below.

5.2. Dynamics. Below we present the results of the stochastic model for the dynamics of PMMA chains adsorbed on aluminum surfaces. A qualitative discussion is given first; a quantitative characterization follows. We have examined both isotactic and syndiotactic polymers over a wide range of temperatures. Results for the two tacticities share many qualitative features, although there are quantitative differences. The results for the two tacticities are presented together to facilitate the comparison between the two chain architectures. In all cases for which data are presented, the number of segments, N, is 1000. The effect of chain length has not been investigated systematically. Preliminary investigations revealed only a minor effect of chain length on the results discussed below, indicating that the infinite chain length limit is approached at $N = 1000$.

In the discussions that follow, we present results for a wide range of temperatures, many of which cannot be realized experimentally. However, the presentation below will show that the dynamical behavior of the PMMA–aluminum system must be studied over a wide range of temperatures to elucidate the physical mechanisms that determine the behavior at room temperature. Furthermore, the most important quantities for the dynamics of adsorbed chains are the activation energies for conformational transitions and adsorption–desorption events divided by k_BT. Spanning a wide range of temperatures is equivalent to spanning a wide range of activation energies at a fixed temperature. Thus, the dynamical behavior of the PMMA–aluminum system at high temperatures may show qualitative similarities to more weakly interacting polymer–solid systems at room temperature. For emphasis throughout the text below, when we quote a given temperature, we also specify the quantity E_a/k_BT, where $E_a = 50$ kJ mol^{-1} is a representative activation energy both for the adsorption of PMMA segments and for conformational transitions between different adsorbed configurations. This activation energy is the most appropriate one to renormalize the temperature scale because the two most important events in the dynamics of adsorbed PMMA are the adsorption of segments and the subsequent conformational relaxation of adsorbed segments.

Qualitative Description. Here we present a qualitative view of the adsorption process for both the isotactic and syndiotactic chains at a low temperature, 300 K ($E_a/k_BT \approx 20$), and a high temperature, 2000 K ($E_a/k_BT \approx 3$). The dynamics of adsorbed polymer chains are followed by accumulating statistics for the time evolution of several quantities of interest: the number of polymer segments in each discrete sorption state, the number of individual adsorption–desorption events occurring in a given time interval, and the average train length of the adsorbed chains. These quantities are plotted in Figures 3–5. Because of the wide range of time scales, all time axes are logarithmic. The data presented in Figures 3–5 are averages over 100 realizations of the adsorption process. The initial adsorbed configurations were generated by randomly placing 5% of the segments in each of the three adsorbed states; the remaining 85% were then free segments in loops and tails.

Consider first the adsorption of an isotactic chain at 300 K. A striking feature of the adsorption processs is the presence of a wide range of time scales. Several distinct time regimes are apparent from the evolution of the sorption state populations, shown in Figure 3a, and the distribution of individual adsorption–desorption events, shown in Figure 4a. At times less than 10^{-8} s, the number of free segments remains nearly constant while the number of segments with only one functional group adsorbed decreases. Thus, most events in this period involve conformational transitions among segments that were initially adsorbed; typically, the segments with only one functional group adsorbed are able to adsorb the second group. After 10^{-8} s, the number of free segments falls drastically; concomitantly, the number of strongly adsorbed segments (those with both functional groups adsorbed) and the average train length, shown in Figure 5a, grow rapidly. In this time regime, the loops and tails are adsorbing to the surface.

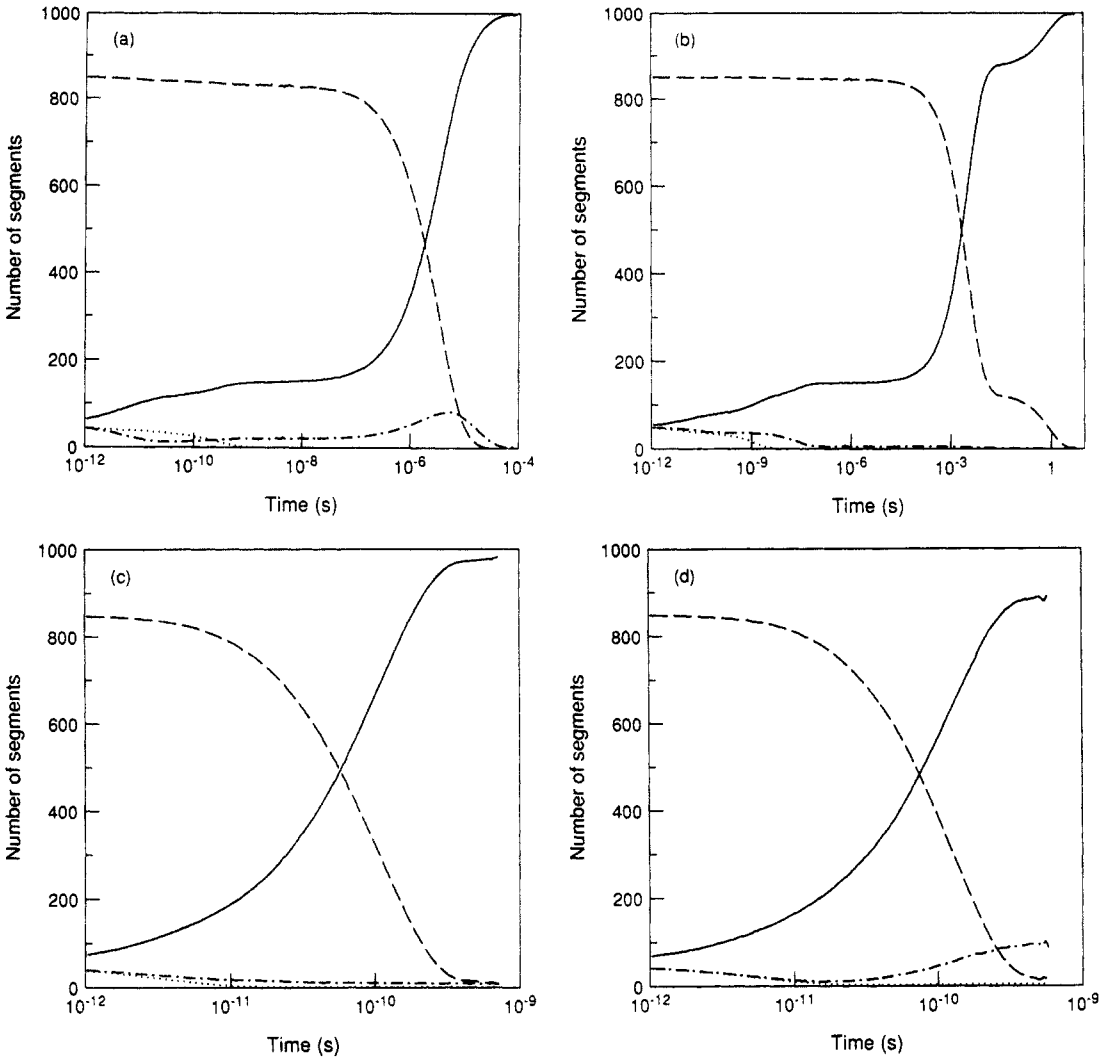

Figure 3. Time evolution of the discrete-state populations for PMMA chains of 1000 segments adsorbed on an aluminum surface: (a) isotactic chain at 300 K; (b) syndiotactic chain at 300 K; (c) isotactic chain at 2000 K; (d) syndiotactic chain at 2000 K. At 300 K, $E_a/k_BT \approx 20$; at 2000 K, $E_a/k_BT \approx 3$. See the text for the discussion of renormalizing the temperature scale with the activation energy E_a. Dotted line: carbonyl group adsorbed, ester oxygen atom desorbed. Dot-dashed line: ester oxygen atom adsorbed, carbonyl group desorbed. Solid line: both adsorbed. Dashed line: neither adsorbed.

Closer examination of the adsorption simulations and the transition probabilities $R_L(Q_i \rightarrow Q'_i|Q_{i-1},Q_{i+1})$ and $R_{NL}(Q_i \rightarrow Q'_i|\mathbf{Q})$ has revealed that the adsorption of loops and tails occurs through a cooperative dynamical process. Qualitatively similar behavior has been seen in previous kinetic Ising models of polymer adsorption.[8] The cooperativity arises because the adsorption rate of an individual segment is greatly enhanced if one of its nearest neighbors is already adsorbed. In other words, the adsorption of a given segment is kinetically constrained until one of its neighbors adsorbs. For example, in the isotactic chain at 300 K, the rate constant R_L for the adsorption of a desorbed segment (into a configuration with both chemisorbing functional groups adsorbed) is 1.72×10^6 s^{-1} when one neighbor is strongly adsorbed and the other neighbor is desorbed; the rate constant is 0.630 s^{-1} when both neighbors are desorbed. Both local and nonlocal effects account for this difference of 6 orders of magnitude. The important factors at the local level include not only torsional strain and nonbonded interactions between monomers but also the activation barrier to chemisorption of the strongly interacting functional groups. Once one segment is adsorbed to the surface, it can help to "pull" its neighbor over the activation barrier. (One could imagine that, for a polymer with a bulky side group, like polystyrene, an adsorbed segment could actually hinder the adsorption of its neighbors because of blocking by the side group.) There is also a nonlocal effect due to the change in configurational entropy that accompanies the adsorption of a segment in a loop. It can be seen from eqs 9 and 10 that the entropic penalty for adsorbing a loop or tail segment is least for the anchoring segments of the loop or tail (the segments nearest to the surface and adjacent to a train). Thus, the nonlocal rate constant $R_{NL}(Q_i \rightarrow Q'_i|\mathbf{Q})$ will be greatest for the anchoring segments of loops and tails. The facilitation of the adsorption process through nearest-neighbor interactions was postulated in the kinetic Ising models of strongly interacting polymers;[8] here that postulate is verified directly from the potential energy surface. We will return to the discussion of the effects of kinetic constraints on the dynamics of adsorbed chains in the next section. Because of the kinetic constraints, the predominant events in the time period from 10^{-7} to 10^{-5} s are the adsorption of free segments that are at the beginning of loops and tails. Pictorially, the adsorption of a long tail can be described as a "zippering" process: if the first segment of a tail is number 980, say, the most probable sequence of adsorption events within the tail will be 980, 981, ..., 999, 1000. Other events may occur during this time period, however, in the other tail or in other loops along the chain.

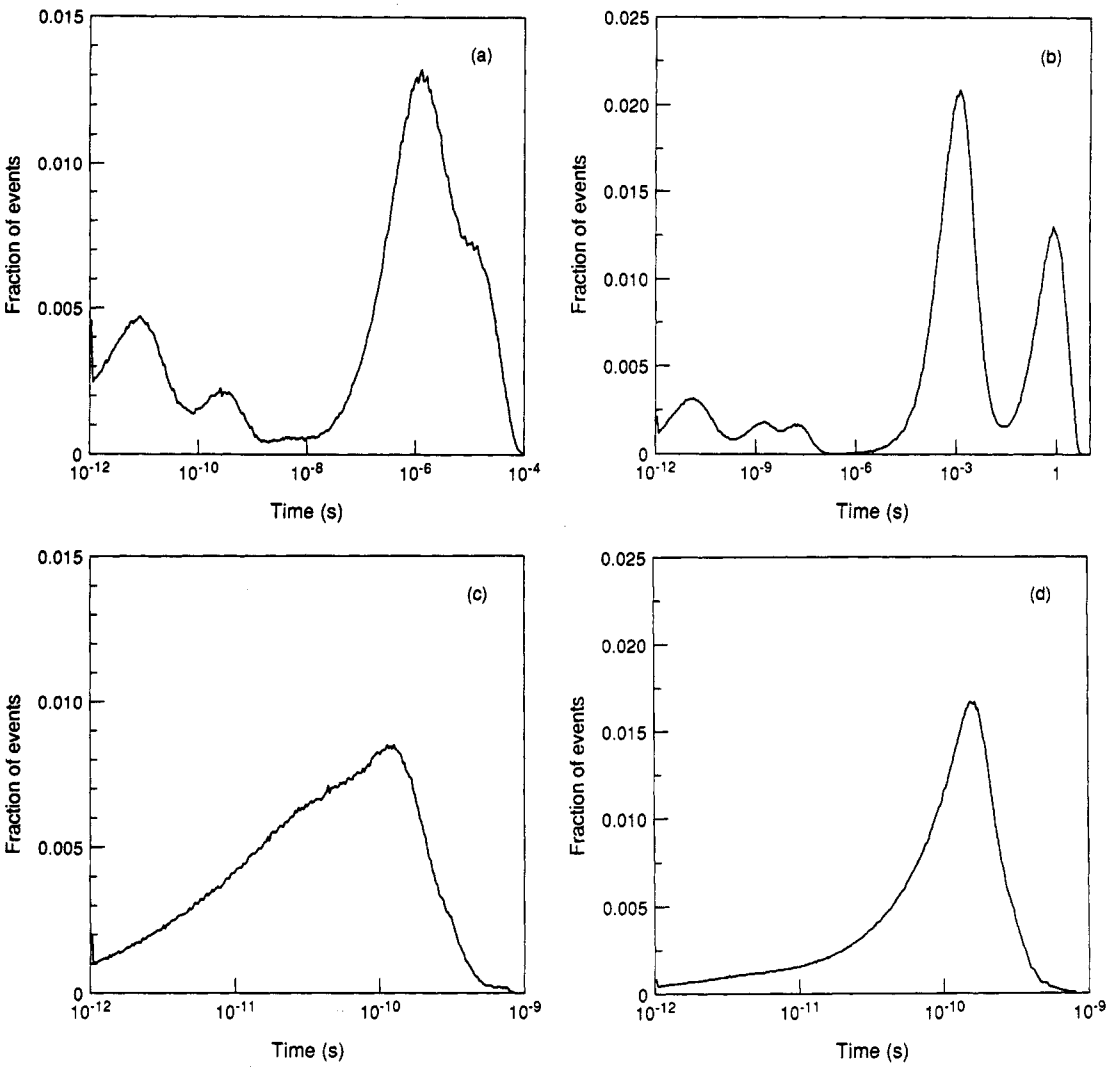

Figure 4. Fractional distribution of individual adsorption–desorption events for PMMA chains of 1000 segments adsorbed on an aluminum surface: (a) isotactic chain at 300 K; (b) syndiotactic chain at 300 K; (c) isotactic chain at 2000 K; (d) syndiotactic chain at 2000 K. At 300 K, $E_a/k_BT \approx 20$; at 2000 K, $E_a/k_BT \approx 3$. See the text for the discussion of renormalizing the temperature scale with the activation energy E_a.

The final stage of the dynamics at low temperatures, from 10^{-5} s onward for the isotactic chain at 300 K, occurs through a mechanism different from the one described above. As noted above, the intermediate stage of the adsorption of loops proceeds from the two anchoring segments (at the termination of trains) to the interior. As a result, in the final stage of adsorption, the polymer chain configuration will be comprised of several long trains with a few isolated desorbed (free) segments. These free segments are the remnants of loops that have adsorbed all but one of their original members. At low temperature, each loop that is present in the initial configuration will ultimately leave one of these "loop remnants". When only one free segment of the loop remains, the mechanism of the adsorption changes. Although the adsorption of a segment is facilitated when *one* of its nearest neighbors is already adsorbed, we find that the adsorption is hindered when *both* nearest neighbors are adsorbed. Again, this verifies an assumption of the kinetic Ising models of adsorbed chain dynamics,[8] that steric hindrance and torsional strain retard adsorption rates when both neighbors are adsorbed. For the isotactic PMMA chain, we find the following sequence of events to be most likely for adsorption of the loop remnants:

...,3,3,4,3,3,... → ...,3,3,2,3,3,... → ...,3,3,3,3,3,...

where the integers are the labels assigned to the discrete states in section 2, and the dots imply that the polymer chain continues in both directions. The presence of the segments with only the ester oxygen atom adsorbed (state 2) as an intermediate causes the maximum in the segment population of that state at 10^{-5} s that can be seen in Figure 3a.

The dynamics of adsorbed syndiotactic PMMA at 300 K share several of the qualitative features found for isotactic PMMA. The event distribution for the syndiotactic PMMA, in Figure 4b, shows several distinct time regimes that are very well separated. At times less than 10^{-7} s, the events correspond to conformational rearrangement of segments that were initially adsorbed. Virtually no events occur for 2 decades in time, until the adsorption of loops and tails begins around 10^{-4} s. The onset of loop and tail adsorption is seen in the sharp rise of the average train length (Figure 5b) and the number of strongly bound segments and the sharp decrease of the number of free segments (Figure 3b). The adsorption of loops and tails for syndiotactic PMMA proceeds in the manner described for isotactic chains. After the zippering process of loop and tail adsorption is nearly complete by 10^{-2} s, there is another lag in the adsorption events until the loop remnants relax to the strongly adsorbed states. The lag can be seen clearly in the event distribution; it is also evident in the plateaus of the segment populations and

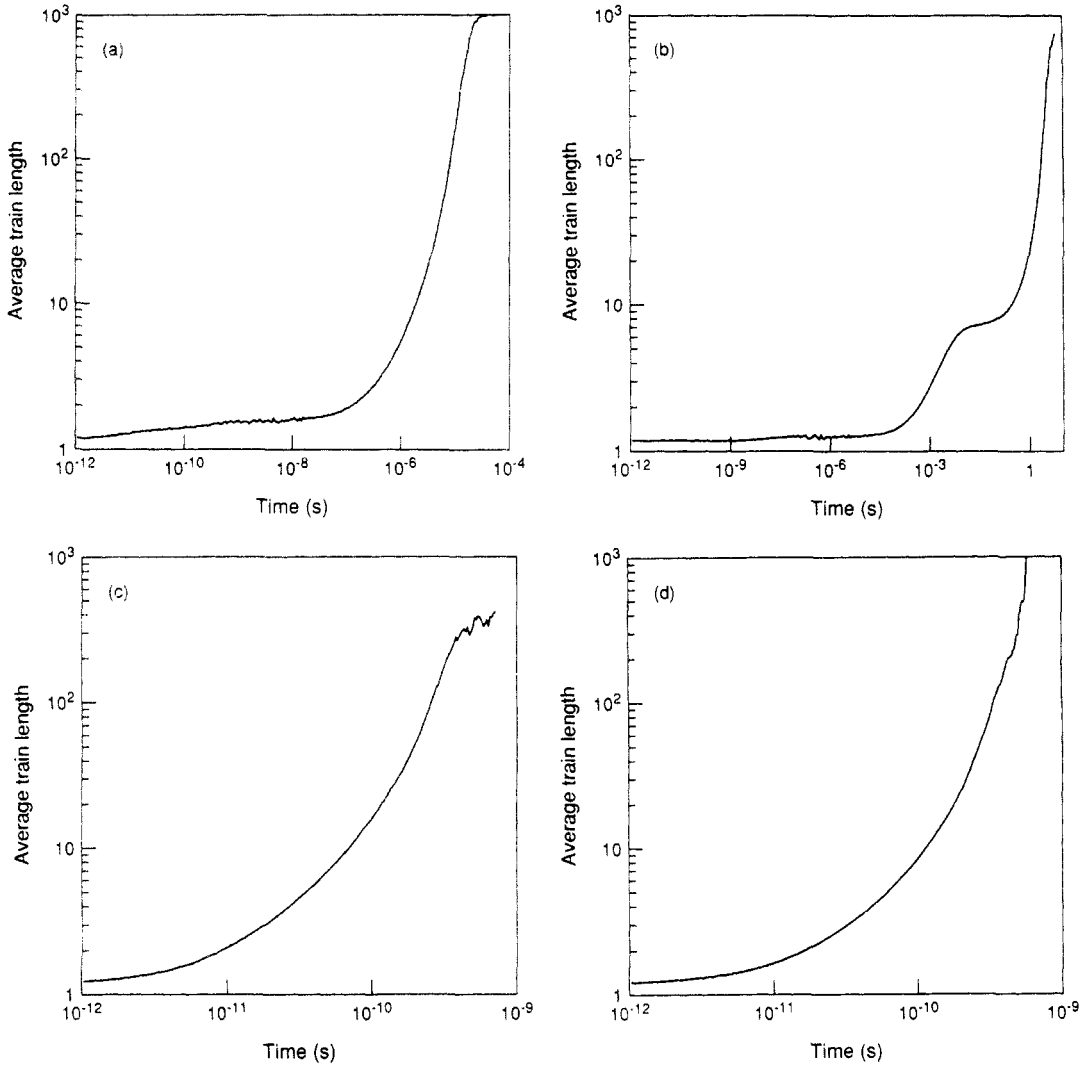

Figure 5. Time evolution of the average train length for PMMA chains of 1000 segments adsorbed on an aluminum surface: (a) isotactic chain at 300 K; (b) syndiotactic chain at 300 K; (c) isotactic chain at 2000 K; (d) syndiotactic chain at 2000 K. At 300 K, $E_a/k_BT \approx 20$; at 2000 K, $E_a/k_BT \approx 3$. See the text for the discussion of renormalizing the temperature scale with the activation energy E_a.

average train length. With the syndiotactic PMMA chain, we find two important paths for the relaxation of the loop remnants:

...,3,3,4,3,3, ... → ...,3,3,1,3,3, ... → ...,3,3,3,3,3, ...

and

...,3,3,4,3,3, ... → ...,3,3,2,3,3, ... → ...,3,3,3,3,3, ...

The second steps in the paths above are so fast, however, that there is no observable increase in the number of segments occupying states 1 and 2. Hence, there is no maximum in the populations of the intermediate states as seen for the isotactic chain.

The dynamics of adsorbed chains at higher temperatures are very different from the dynamics at low temperatures. Parts c and d of Figures 3–5 present the data for isotactic and syndiotactic PMMA chains adsorbing at 2000 K. Although the high temperature is unrealistic for PMMA chains, we focus on the quantity E_a/k_BT discussed above; at 2000 K, $E_a/k_BT \approx 3$. This value is representative of a more weakly interacting physisorbed polymer at room temperature. As expected, at a higher temperature, the adsorption is much faster; it is complete in less than 10^{-9} s. There are no distinct time regimes, however, as seen by the broad event distributions in parts c and d of Figure 4. The segment populations and the average train length also change gradually; the adsorption of loops and tails through the zippering process and the subsequent relaxation of loop remnants are no longer the predominant dynamical mechanisms. At the higher temperatures, the effects of the activation barriers to adsorption and desorption events are greatly reduced; the kinetic constraints are not severe, and the dynamics are much less cooperative. This point is expanded in the discussion below.

Quantitative Characterization. The qualitative features of the dynamics of PMMA chains adsorbed on aluminum show a degree of cooperativity during the adsorption of loops and tails at low temperatures. The phenomenological kinetic Ising models for adsorbed chain dynamics[8] also show that dynamical behavior is cooperative and is similar to that observed for glass-forming liquids. Experimental evidence of similarities between adsorbed polymers and structural glasses also exists.[9] One major purpose of the present work is to examine the dynamical behavior of a real polymer–solid interface without making assumptions about the nature of the interactions. The goal is to verify the existence of the glasslike behavior that the phenomenological models predict[8] and, more importantly, to examine the microscopic origins of the cooperative dynamics.

In order to characterize the dynamics of adsorbed polymers quantitatively, we have focused on the nonlinear

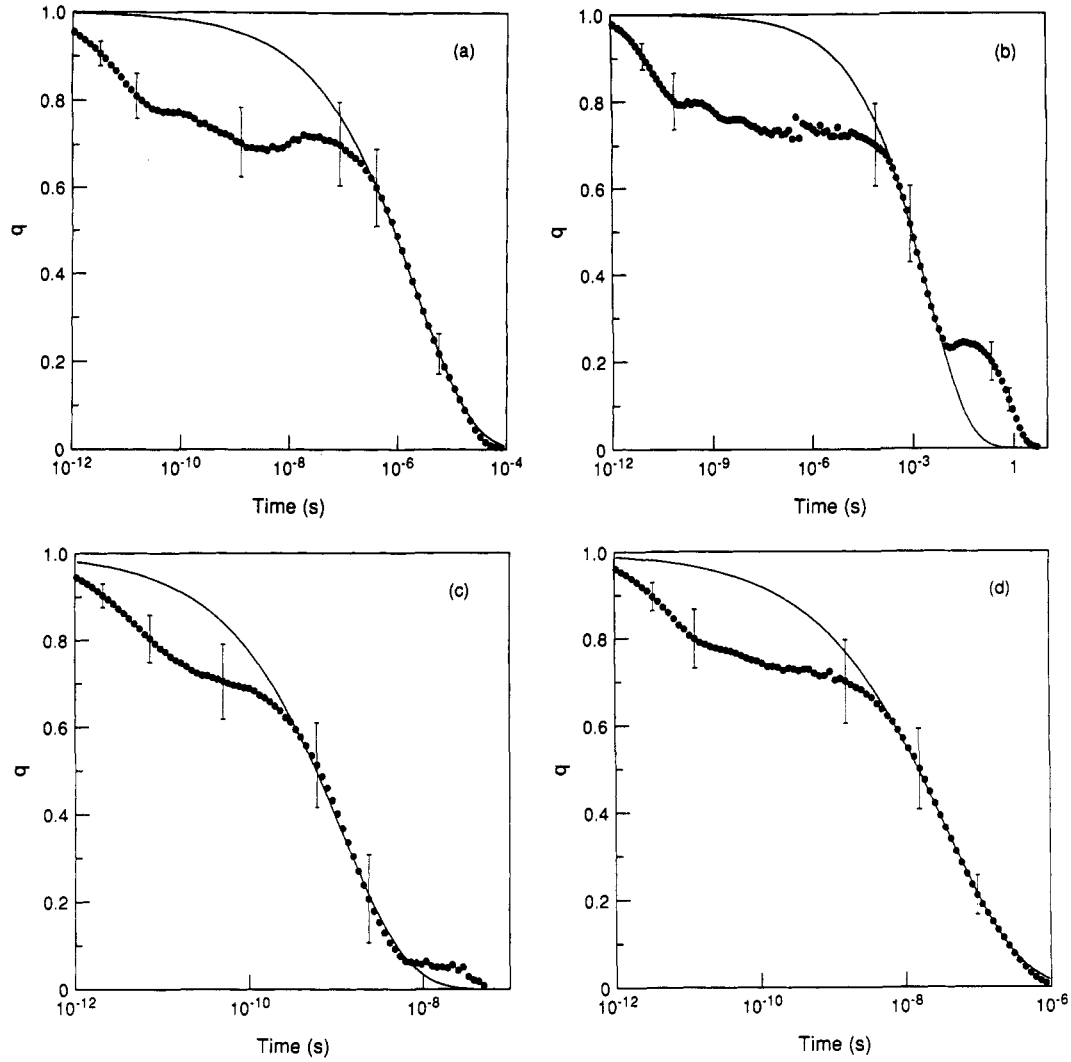

Figure 6. Time evolution of the relaxation function defined by eq 25 for PMMA chains of 1000 segments adsorbed on an aluminum surface. The data from the stochastic simulations (●) are averages over 1000 realizations using independent initial configurations; error bars denote 1 standard deviation of the data. Solid lines are fits to eq 1. The parameters β and τ_{KWW} were determined through a weighted nonlinear least-squares fit of the relaxation function:[47] (a) isotactic chain at 300 K, $\beta = 0.412$, $\tau_{KWW} = 2.06 \times 10^{-6}$ s; (b) syndiotactic chain at 300 K, $\beta = 0.358$, $\tau_{KWW} = 2.71 \times 10^{-3}$ s; (c) isotactic chain at 667 K, $\beta = 0.562$, $\tau_{KWW} = 1.13 \times 10^{-9}$ s; (d) syndiotactic chain at 667 K, $\beta = 0.425$, $\tau_{KWW} = 3.55 \times 10^{-8}$ s.

relaxation function, $q(t)$, for the strongly adsorbed segments:

$$q(t) = \frac{n(t) - n_{eq}}{n(0) - n_{eq}} \tag{25}$$

where $n(t)$ is the number of strongly adsorbed segments (those with both chemisorbing functional groups adsorbed) at time t and n_{eq} is the number of strongly adsorbed segments at equilibrium. The relaxation function is normalized to unity at $t = 0$ and decays to zero if the system evolves to equilibrium. Since we are examining a nonequilibrium process, $q(t)$ is not temporally homogeneous; i.e., the time origin in eq 25 cannot be shifted arbitrarily as it can be in equilibrium systems. We also calculate the corresponding nonlinear relaxation time, τ^{nl}, of the strongly adsorbed segments:

$$\tau^{nl} = \int_0^\infty q(t)\, dt \tag{26}$$

It is appropriate to define the relaxation time based on the strongly adsorbed segments because the slowest events in the adsorption process, the relaxation of loop remnants discussed above, involve transitions into the strongly adsorbed state. Thus, τ^{nl} is a measure of the longest relaxation time.

The relaxation function $q(t)$ and the relaxation time τ^{nl} depend on the initial configuration of the polymer chain. Accordingly, its computation requires averages over many initial configurations and many realizations of the stochastic dynamics. In the results presented below, the initial configuration space was sampled extensively by accumulating averages from 1000 independent initial conditions. For each starting configuration, the total fraction of initially adsorbed segments was chosen randomly from a uniform distribution between 0.05 and 0.50; each of the three adsorbed states was equally likely.

The evolution of the relaxation function for isotactic and syndiotactic PMMA at 300 and 667 K is shown in Figure 6. At 667 K, the normalized activation energy $E_a/k_BT \approx 9$. The behavior of $q(t)$ mirrors the qualitative features of the adsorption that were discussed above. The different time regimes are evident for both tacticities and both temperatures. At first, the initially adsorbed segments relax quickly into the strongly adsorbed configurations; this is responsible for the decrease of q from unity to roughly 0.75. A plateau region of very little activity follows for several decades in time.[39] The sharp decrease of q following the plateau region corresponds to the second stage, adsorption of loops and tails. By far the most adsorption events occur in this region where q decreases

from 0.75 to 0.25. The final stage, in which the loop remnants relax, is especially apparent in Figure 6b because the time regions are very well separated. (See the event distributions of Figure 4b.)

An important result of the quantitative characterization is that the decay of the relaxation function is not purely exponential in time. Except for the very first and last periods of adsorption, the relaxation function can be described by the stretched-exponential or Kohlrausch–Williams–Watts (KWW) function given in eq 1. (Note that τ_{KWW} is not equivalent to the nonlinear relaxation time τ^{nl}.) The KWW function fits the relaxation function well only in the time range that corresponds to the adsorption of loops and tails (the overwhelming majority of events). In the time regions where the fit is not satisfactory, the physical mechanisms that lead to adsorption are different. In the initial time period the dominant events are local conformational rearrangements, and in the final time period the dominant events are the adsorption of loop remnants.

The nonexponential relaxation that we observe over a wide range of temperatures is a direct consequence of the kinetic constraints that are operative during the adsorption of the loops and tails. The stretching parameter β in eq 1 is a rough indicator of the severity of the kinetic constraints. (See the discussion below.) Therefore, it is instructive to examine how the stretching parameter varies as a function of temperature. The variation of β with inverse temperature is shown in Figure 7 for both isotactic and syndiotactic chains. The values of β nearly coincide for the two tacticities at the highest and lowest temperatures but differ at intermediate temperatures. At the highest temperature, where $E_a/k_BT \approx 1$, the values of β are rather large, around 0.75. At infinite temperature, one expects that β would asymptotically approach unity (Debye relaxation). As the temperature is lowered, the values of β decrease until they finally plateau near 0.35 for temperatures below 300 K ($E_a/k_BT > 20$).

The results presented above show that the dynamical behavior of PMMA chains adsorbed on aluminum is qualitatively similar to that observed for structural glasses. Thus, we expect that the physical mechanisms responsible for the dynamical features of strongly adsorbed polymers are similar to those present in structural glasses. It has been shown that dynamical constraints give rise to nonexponential relaxation;[40-42] these constraints generally result from rugged potential energy or free energy surfaces.[12,43] PMMA chains adsorbed on aluminum and structural glasses share both of these features: rugged energy surfaces and strong kinetic constraints. In previous kinetic Ising models of bulk polymers,[17] adsorbed polymers,[8] and structural glasses,[44] dynamical constraints were introduced explicitly without making a detailed connection to their microscopic origin. In other words, the kinetic constraints that are operative were not derived explicitly from the microscopic Hamiltonian. Nevertheless, the fact that these models reproduce the qualitative features found in real polymers and glass-forming liquids enforces the idea that dynamical constraints are responsible for the glassy dynamics. For the strongly adsorbed PMMA chains, however, the microscopic origins of the dynamical constraints are much clearer. For PMMA adsorption at low temperatures, strong kinetic constraints are in effect during the adsorption of loops and tails. As discussed above, the adsorption rate of a PMMA segment is greatly affected by its nearest neighbors and entropic penalties imposed by the surface upon adsorption of segments further along the chain. As a consequence, the dynamics of the adsorbed

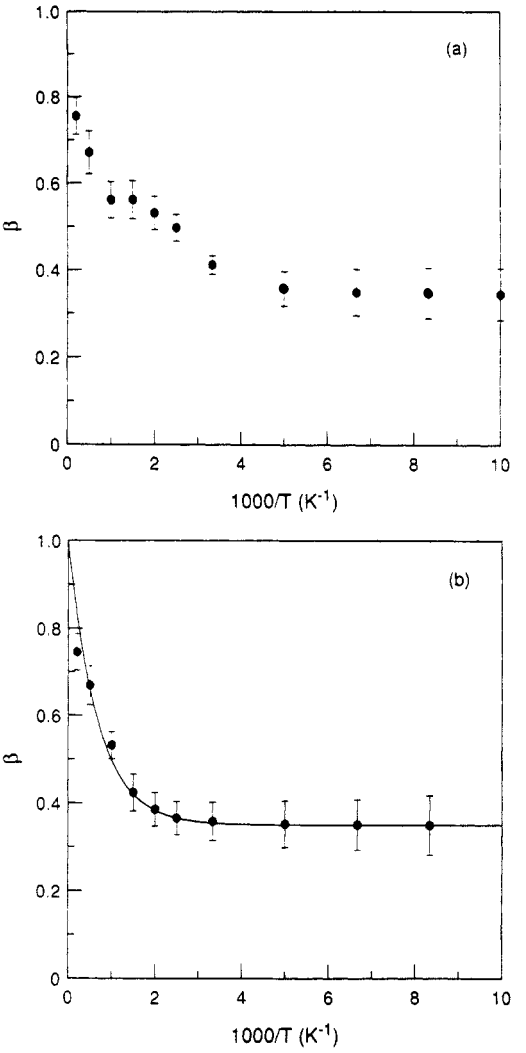

Figure 7. KWW stretching parameter β (●) versus inverse temperature. Error bars indicate 1 standard deviation of the fitted parameter:[47] (a) isotactic chain; (b) syndiotactic chain. The solid line in (b) is the function $\beta = 0.35 + 0.65 \exp(-1480/T)$.

chains are highly cooperative. For instance, before a segment near the end of a tail or the middle of a loop has a significant chance to adsorb at low temperatures, all of the segments preceding it back to the anchoring segment must adsorb.

The role of the dynamical constraints in strongly adsorbed polymers can also be seen by considering their effect on the topology of the configuration space of the adsorbed polymer.[11,41,42] The polymer dynamics can be described by the time evolution of the configuration point **Q** among the 4^N discrete points in configuration space. The transition rates between configuration space points are governed by the structure of the free energy surface, i.e., the adsorption energetics and the conformational and configurational changes that accompany adsorption–desorption events. The strong and orientation dependent segment–surface energetics lead to kinetic bottlenecks for conformational and configurational transitions that must occur for relaxation to the equilibrium adsorbed state. For the PMMA–aluminum system at low temperatures, many transitions between points in the configuration space are essentially forbidden. In effect, the kinetic constraints reduce the available paths between points in configuration space to a sparsely connected network. Relaxation to equilibrium then must follow a tortuous route through the configuration space. This is the origin of the cooperative dynamics that we observe. Computer simulations

of several models with restricted paths through configuration space do show the effects of kinetic constraints through nonexponential relaxation.[41,42,45] In the PMMA–aluminum system, the kinetic bottlenecks which arise naturally from the free energy surface and which lead to cooperative dynamical behavior also lead to nonexponential relaxation.

It is interesting to consider what physical significance to attach to the stretching parameter β in the KWW function. Intuitively, one expects that the value of β is a rough indicator of the severity of the kinetic constraints, or the degree to which they are operative in a given situation. The decrease of β with temperature can be interpreted in this way. At high temperatures, the kinetic constraints involved in loop and tail adsorption are not as important because the features of the potential energy surface that give rise to the constraints become small in comparison to the thermal energy, k_BT. As the temperature is lowered, energy barriers for many adsorption pathways become significantly larger than k_BT. These pathways are then effectively eliminated as possible routes to relaxation, and more cooperative motions are required. The plateau of β below 300 K indicates that the kinetic constraints are fully operative at 300 K ($E_a/k_BT \approx 20$); lowering the temperature has no further observable effect on the severity of the constraints. Similar behavior has been seen in a simplified model of glassy relaxation.[45] The diffusive motion of a random-walker on a hypercube with randomly deleted vertices has been described with the KWW function; the value of β decreases from unity to roughly $^1/_3$ as the network of paths becomes increasingly sparse.[45]

The temperature dependence of the nonlinear relaxation times is also important for relating the dynamics of adsorbed polymers to dynamics in glass-forming liquids. At each temperature, a relaxation time was calculated from eq 26 for each of the 1000 independent realizations of the adsorption process. The upper limit of integration was the time required for the relaxation function to decay to 0.001; this corresponds to the relaxation of all but one segment in the chains of 1000 segments. The variations of the nonlinear relaxation times with temperature are shown in the Arrhenius plots of Figure 8. For a simple relaxation process with a single significant activation energy E_{Arr}, the relaxation time should follow the Arrhenius expression of eq 3. For the syndiotactic chain, Arrhenius behavior is seen at all temperatures below 1000 K ($E_a/k_BT \approx 6$). For the isotactic chain, the temperature dependence is non-Arrhenius at high and intermediate temperatures but reverts to Arrhenius behavior at temperatures below 200 K ($E_a/k_BT \approx 30$). From the slopes of the lines in Figure 8, the apparent activation energy E_{Arr} is estimated to be 42 kJ mol^{-1} for isotactic PMMA and 67 kJ mol^{-1} for syndiotactic PMMA. These values are within the range of the "baseline" activation energy, E_a, of 50 kJ mol^{-1} that has been used to normalize the temperature scale.

Although the behavior at low temperatures is Arrhenius, it should be emphasized that the relaxation times at the lowest temperatures are beginning to surpass experimental time scales. For the isotactic chain at 100 K, for example, τ^{nl} is approximately 33 years. As a result, experiments that cannot access these time scales will conclude that the relaxation times have diverged, corresponding to a dynamical falling out of equilibrium and the strongly non-Arrhenius behavior suggested by the Vogel–Fulcher form of eq 2. In fact, the relaxation times for the isotactic chain above 200 K can be fit well by the Vogel–Fulcher form with the parameters E_{VF} = 25 kJ mol^{-1}, $\tau_{VF} = 7.3 \times 10^{-12}$ s, and T_{VF} = 75 K. While we know that the true behavior below 200 K is Arrhenius, the long relaxation times might not be accessible to experiments or detailed computer simulations. Without the knowledge of the relaxation times at lower temperatures, the fact that the data are consistent with the Vogel–Fulcher equation might be interpreted as foreshadowing a real divergence at T_{VF} = 75 K.

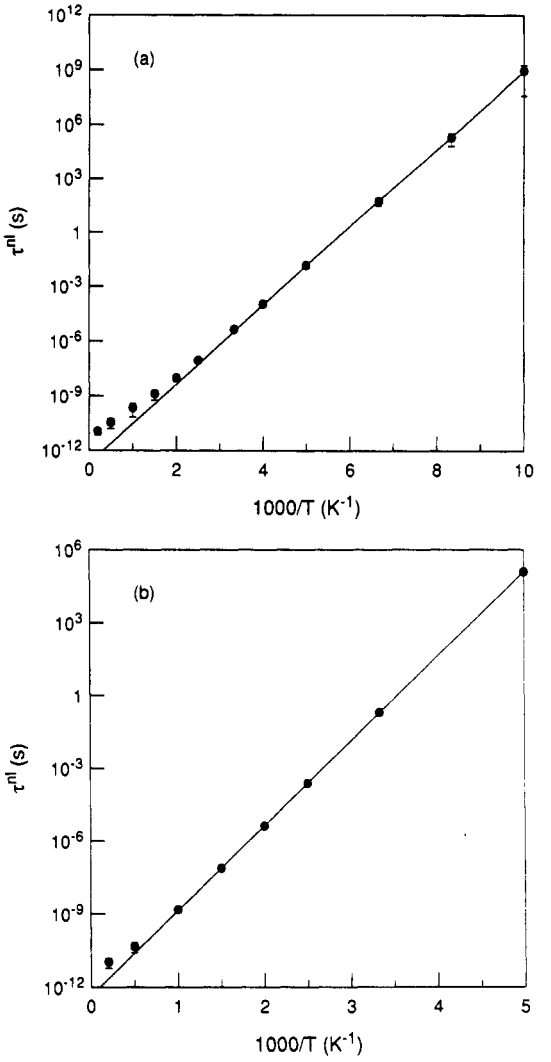

Figure 8. Arrhenius plot of the nonlinear relaxation times, τ^{nl}, defined by eq 26. The data from the stochastic simulations (●) are averages over 1000 realizations; error bars denote 1 standard deviation of the data. Solid lines are fits to the Arrhenius form, eq 3, using the relaxation times at temperatures 300 K and below: (a) isotactic chain, E_{Arr} = 42 kJ mol^{-1}; (b) syndiotactic chain, E_{Arr} = 67 kJ mol^{-1}.

The temperature dependence of the relaxation times for isotactic PMMA in the non-Arrhenius region indicates that the apparent activation energy for relaxation,

$$E^*(T) = \frac{d(\ln \tau^{nl})}{d(1/T)} \tag{27}$$

is increasing as the temperature is lowered from 2000 to 300 K (as E_a/k_BT increases from 3 to 20). The increase in the apparent activation energy has two separate causes. First, the local transition probabilities, $R_L(Q_i \rightarrow Q'_i | Q_{i-1}, Q_{i+1})$, decrease with decreasing temperature. This is a general feature of systems with rugged potential energy surfaces.[12,13] According to eq 8, each transition path from one macrostate to another is weighted by the probability of the microstate originating the transition being occupied. As the temperature is lowered, fewer microstates will be

occupied with a significant probability, so the number of paths contributing to the overall transition probability will decrease. This reflects an entropic restriction at the level of individual polymer segments (unrelated to the entropic constraints imposed by the surface) that grows more severe as the temperature is lowered. Furthermore, one expects the low energy microstates (which will be occupied preferentially as the temperature is lowered) to have higher activation energies for significant conformational transitions (those that change the adsorption state). So not only are the number of transition paths reduced as the temperature is lowered but also the paths with the highest activation energies are likely to be the ones of importance. Second, as discussed above, the topology of the polymer configuration space changes with temperature. At higher temperatures, relaxation can proceed by many routes in addition to the zippering of loops and tails described above. As the temperature is lowered, however, the kinetic constraints become active, and many paths in configuration space become kinetically blocked. This rarefaction of the accessible paths in configuration space is equivalent to a gradual increase in entropic barriers to relaxation on the scale of the configuration space of the entire polymer chain. As the paths become blocked, more cooperativity is required for relaxation to equilibrium. As in other systems with strong kinetic constraints,[41,42,44,46] the requirement for cooperative dynamics over long length scales leads to non-Arrhenius behavior.

In contrast to the non-Arrhenius temperature dependence for the isotactic chain at high temperatures, the region of Arrhenius dependence indicates that the character of the final stage of relaxation differs from that of the region in which stretched-exponential relaxation is observed. The Arrhenius behavior at low temperatures reflects the nature of the final stage of the relaxation, the adsorption of loop remnants. Since τ^{nl} is a measure of the *longest* relaxation time of the adsorbed chains, at low temperatures its behavior is dominated by the slowest dynamical process, the adsorption of loop remnants. Since the loop remnants are spatially separated along the polymer chain, they relax independently of each other; cooperative motions over large length scales, which often lead to non-Arrhenius behavior, are not required in the final stage of relaxation. Furthermore, at low enough temperatures, the single dynamical pathway (with a single activation energy) that corresponds to relaxation of loop remnants is the rate-limiting step in the relaxation process; the activation energy for that pathway is the energy E_{Arr} that appears in eq 3.

Many of the phenomenological features of the dynamics of strongly adsorbed polymers have been demonstrated through competitive adsorption experiments. Johnson and Granick[9] have studied the kinetics of the displacement of polystyrene (PS) on oxidized silicon by PMMA. The desorption kinetics were described well by a KWW function, eq 1, in which both β and τ_{KWW} were temperature dependent. The value of β increased from 0.5 at 25 °C to 0.6 at 50 °C. The temperature dependence of τ_{KWW} was clearly non-Arrhenius; the time required for desorption exceeded experimental time scales below 25 °C. The experimental situation of competitive adsorption is somewhat different than the case of adsorption from dilute solution treated here. We expect, however, that the underlying idea that glassy dynamics results from strong kinetic constraints is still applicable. As discussed by Johnson and Granick, for PS chains to desorb from the surface, they must diffuse through a network of "cages" formed by the strongly adsorbed PMMA chains and the impenetrable surface. In other words, the partially adsorbed PMMA chains provide topological obstacles that impede the desorption of PS chains. As a result, the kinetic constraints themselves evolve in time as the PMMA chains relax toward equilibrium; the theoretical treatment of competitive adsorption would necessarily be more complicated than the analysis presented here.

6. Conclusions

We have presented a stochastic model for the dynamics of PMMA chains adsorbed on an aluminum surface. The model can investigate the length scales and time scales relevant to polymer adsorption by employing a coarse-grained representation of the polymer chain (in terms of discrete adsorption states) and stochastic dynamics. Previous kinetic Ising models of polymer dynamics[8,17] have also used discrete-state representations of polymer configurations. The model presented here differs from the kinetic Ising models in two respects. In the present model, polymer segments are classified into four discrete states, rather than the two-state classification used in Ising models. The crucial distinction of the present model, however, is that the dynamical rules are not phenomenological but are derived directly from the potential energy surface. In the kinetic Ising model of adsorbed polymer dynamics,[8] kinetic constraints operating between neighboring segments were postulated based on physical induction. In particular, the authors assumed that the adsorption rate of a particular segment along the chain would be enhanced if one of its nearest neighbors was already adsorbed. Here, adsorption rate constants calculated from the potential energy surface yielded the same qualitative features of the kinetic constraints that were used in ref 8. This finding verifies that the qualitative behavior of the kinetic Ising model illustrates general features of strongly interacting polymer–solid interfaces.

By incorporating the details of the PMMA–aluminum potential energy surface, the stochastic model has been able to investigate the effects of tacticity on the adsorbed chain dynamics. There are many qualitative similarities between the dynamics of isotactic and syndiotactic PMMA chains adsorbed on aluminum; nevertheless, the stochastic model predicts several quantitative effects of tacticity. At temperatures below 500 K, relaxation times for syndiotactic chains are several orders of magnitude greater than those for isotactic chains and the apparent activation energy for relaxation of a syndiotactic chain is roughly 1.5 times that for an isotactic chain.

The dynamics of PMMA adsorbing on aluminum are qualitatively similar to the dynamics of glass-forming liquids. Both systems exhibit nonexponential relaxation and non-Arrhenius temperature dependences of relaxation times. The common features are rugged energy surfaces and strong kinetic constraints. While the exact microscopic basis of the kinetic constraints in glass-forming liquids remains unclear, the present stochastic model has clarified the origins of the kinetic constraints for PMMA chains adsorbed on aluminum. For strongly adsorbed polymers, the kinetic constraints have several physical origins: (1) nearest-neighbor interactions; (2) strong and specific segment–surface interactions; (3) entropic constraints introduced by an impenetrable surface; (4) topological barriers due to other adsorbed chains; and (5) competition for surface sites. The first two effects depend on the details of the interaction potential, and thus the specific chemical constitution of the polymer segments and the substrate; the other effects are generic to all polymer systems. Topological constraints are responsible

for the "caging" effect described by Johnson and Granick[9] for the glassy dynamics of PS desorption from a surface in the presence of partially adsorbed PMMA. Similar caging effects should also affect the dynamics of PMMA adsorption from concentrated solutions onto initially bare surfaces because segments in loops and tails cannot diffuse freely to the surface in the presence of other partially adsorbed polymers. Competition for surface sites may also provide significant kinetic constraints. Once a large fraction of the surface is covered with adsorbed segments, a segment still in a short loop or tail may have to wait for adsorbed segments to diffuse in the surface layer and free a surface site. The model presented here explicitly accounts for only the first three effects. Although the last two effects are most important for concentrated solutions and melts, they can also be important for an isolated chain, which may see other parts of itself as obstacles to adsorption and competitors for surface sites. However, the additional complexities should only serve to make the effects that we have observed more pronounced. Work currently underway is aimed at investigating the dynamical consequences of topological constraints and competition for surface sites.

Acknowledgment. This material is based on work supported under a National Science Foundation Graduate Fellowship awarded to J.S.S. A.K.C. thanks the Shell Foundation, the Dexter Corp., and the U.S. DOE Office of Basic Energy Sciences for financial support. Computational resources were provided by the University of California Program in Supercomputing at UCLA. Discussions with W. H. Miller and E. M. Sevick regarding the search for potential energy extrema are gratefully acknowledged.

Appendix

Here we show that the effective rate constants defined by eq 8 satisfy the condition of detailed balance for the macrostate populations. The statement of detailed balance is

$$P_A^{eq} R_{A\to B} = P_B^{eq} R_{B\to A} \tag{28}$$

where P_A^{eq} and P_B^{eq} are the true equilibrium populations of macrostates A and B, respectively. The equilibrium population of macrostate A is given simply by

$$P_A^{eq} = Z_A/Z \tag{29}$$

where Z_A is the local configurational partition function defined by eq 7 and Z (without a subscript) denotes the configurational partition function for the entire configuration space:

$$Z = \int \exp[-V(\mathbf{x})/k_B T]\, d\mathbf{x} \tag{30}$$

The individual rate constants for transitions between microstates satisfy detailed balance among themselves:

$$p_i^{eq} k_{i\to j} = p_j^{eq} k_{j\to i} \tag{31}$$

where p_i^{eq} and p_j^{eq} are the true equilibrium probabilities for microstates i and j:

$$p_i^{eq} = Z^{-1} \int_i \exp[-V(x)/k_B T]\, dx \tag{32}$$

As in eq 6, the integration in the preceding equation is limited to the volume of configuration space enclosing microstate i. By comparing eq 32 with eq 6, the following identities are clear:

$$p_i^A = (Z/Z_A)\, p_i^{eq}, \quad p_j^B = (Z/Z_B) p_j^{eq} \tag{33}$$

The ratio of the macrostate rate constants can be written as follows:

$$\frac{R_{A\to B}}{R_{B\to A}} = \frac{\sum p_i^A k_{i\to j}}{\sum p_j^B k_{j\to i}} \tag{34}$$

where the summations are over all transition between macrostates, as in eq 8. Now substitute the identities from eq 33, yielding

$$\frac{R_{A\to B}}{R_{B\to A}} = \frac{(Z/Z_A)}{(Z/Z_B)} \frac{\sum p_i^{eq} k_{i\to j}}{\sum p_j^{eq} k_{j\to i}} \tag{35}$$

Because the individual rate constants $k_{i\to j}$ satisfy detailed balance, the following equation holds:

$$\sum_{i\leftrightarrow j} p_i^{eq} k_{i\to j} = \sum_{i\leftrightarrow j} p_j^{eq} k_{j\to i} \tag{36}$$

and the ratio of the summations in eq 35 is unity. That leaves

$$\frac{R_{A\to B}}{R_{B\to A}} = \frac{Z_B}{Z_A} = \frac{P_B^{eq}}{P_A^{eq}} \tag{37}$$

in accord with the condition of detailed balance, eq 28.

References and Notes

(1) Scheutjens, J. M. H. M.; Fleer, G. J. *J. Phys. Chem.* **1979**, *83*, 1619; **1980**, *84*, 178.
(2) Eisenriegler, E.; Kremer, K.; Binder, K. *J. Chem. Phys.* **1982**, *77*, 6296.
(3) de Gennes, P.-G. *Adv. Colloid Interface Sci.* **1987**, *27*, 189.
(4) Takahashi, A.; Kawaguchi, M. *Adv. Polym. Sci.* **1982**, *46*, 1.
(5) Cohen-Stuart, M.; Cosgrove, T.; Vincent, B. *Adv. Colloid Interface Sci.* **1986**, *24*, 143.
(6) Shaffer, J. S.; Chakraborty, A. K.; Tirrell, M.; Davis, H. T.; Martins, J. L. *J. Chem. Phys.* **1991**, *95*, 8616.
(7) Chakraborty, A. K.; Shaffer, J. S.; Adriani, P. M. *Macromolecules* **1991**, *24*, 5226.
(8) Chakraborty, A. K.; Adriani, P. M. *Macromolecules* **1992**, *25*, 2470. Adriani, P. M.; Chakraborty, A. K. *J. Chem. Phys.*, in press.
(9) Johnson, H. E.; Granick, S. *Science* **1992**, *255*, 966.
(10) Brawer, S. *Relaxation in Viscous Liquids and Glasses*; American Ceramic Society: Columbus, OH, 1985.
(11) Fredrickson, G. H. *Annu. Rev. Phys. Chem.* **1988**, *39*, 149.
(12) Hoffmann, K. H.; Sibani, P. *Phys. Rev. A* **1988**, *38*, 4261.
(13) Frauenfelder, H.; Sligar, S. G.; Wolynes, P. G. *Science* **1991**, *254*, 1598.
(14) The glassy interfacial layer discussed here should not be confused with a glassy layer near an interface due to increased density, as proposed by: Kremer, K. *J. Phys. (Paris)* **1986**, *47*, 1269. The effects alluded to here are purely kinetic, introduced via strong and specific interactions with the surface, and have no relationship to the glass transition of the bulk polymer.
(15) Chakraborty, A. K.; Davis, H. T.; Tirrell, M. *J. Polym. Sci., Polym. Chem. Ed.* **1990**, *28*, 3185.
(16) As general references for kinetic Ising models, see the following: Glauber, R. J. *J. Math. Phys.* **1963**, *4*, 294. Kawasaki, K. In *Phase Transitions and Critical Phenomena*; Domb, C., Green, M. S., Eds.; Academic Press: London, 1972; Vol. 2.
(17) Other kinetic Ising models for polymer dynamics can be found in the following: Orwoll, R. A.; Stockmayer, W. H. *Adv. Chem. Phys.* **1969**, *15*, 305. Skinner, J. L. *J. Chem. Phys.* **1983**, *79*, 1955. Isbister, D. J.; McQuarrie, D. A. *J. Chem. Phys.* **1974**, *60*, 1937. Budimir, J.; Skinner, J. L. *J. Chem. Phys.* **1985**, *82*, 5232.
(18) Frantz, P.; Granick, S. *Phys. Rev. Lett.* **1991**, *66*, 899.
(19) van Kampen, N. G. *Stochastic Processes in Physics and Chemistry*; North-Holland: Amsterdam, 1981.
(20) Stillinger, F. H.; Weber, T. A. *Phys. Rev. A* **1982**, *25*, 978.
(21) June, R. L.; Bell, A. T.; Theodorou, D. N. *J. Phys. Chem.* **1991**, *95*, 8866.
(22) Hänggi, P.; Talkner, P.; Borkovec, M. *Rev. Mod. Phys.* **1990**, *62*, 251.

(23) Palmer, R. G. *Adv. Phys.* **1982**, *31*, 669.
(24) Chandrasekhar, S. *Rev. Mod. Phys.* **1943**, *15*, 1.
(25) Hoeve, C. A. J. *J. Chem. Phys.* **1965**, *43*, 3007.
(26) Feller, W. *An Introduction to Probability Theory and Its Applications*; Wiley: New York, 1968.
(27) Tsikoyiannis, J. G.; Wei, J. *Chem. Eng. Sci.* **1991**, *46*, 233.
(28) Hoel, P. G.; Port, S. C.; Stone, C. J. *Introduction to Stochastic Processes*; Houghton Mifflin: Boston, 1972.
(29) Vacatello, M.; Flory, P. J. *Macromolecules* **1986**, *19*, 405.
(30) Nicholson, D.; Parsonage, N. G. *Computer Simulation and the Statistical Mechanics of Adsorption*; Academic Press: London, 1982.
(31) de Heer, W. A.; Milani, P.; Châtelain, A. *Phys. Rev. Lett.* **1989**, *63*, 2834.
(32) Cerjan, C. J.; Miller, W. H. *J. Chem. Phys.* **1981**, *75*, 2800.
(33) Chang, G.; Guida, W. C.; Still, W. C. *J. Am. Chem. Soc.* **1989**, *111*, 4379.
(34) Banerjee, A.; Adams, N.; Simon, J.; Shepard, R. *J. Phys. Chem.* **1985**, *89*, 52.
(35) Baker, J. *J. Comput. Chem.* **1986**, *7*, 385.
(36) Rosenberg, R. O.; Berne, B. J.; Chandler, D. *Chem. Phys. Lett.* **1980**, *75*, 162. Montgomery, J. A., Jr.; Holmgren, S. L.; Chandler, D. *J. Chem. Phys.* **1980**, *73*, 3688.
(37) Chandler, D. *J. Chem. Phys.* **1978**, *68*, 2959.
(38) Voter, A.; Doll, J. D. *J. Chem. Phys.* **1985**, *82*, 80.
(39) Even after performing 1000 simulations it is difficult to accumulate good statistics in the region of time between the relaxation of initially adsorbed segments and the adsorption of loops and tails. The poor statistics are responsible for the noisy appearance of the relaxation functions in this region.
(40) Palmer, R. G.; Stein, D. L.; Abrahams, E.; Anderson, P. W. *Phys. Rev. Lett.* **1984**, *53*, 958.
(41) Palmer, R. G. In *Heidelberg Colloquium on Glassy Dynamics*; van Hemmen, J. L., Morgenstern, I., Eds.; Springer-Verlag: Berlin, 1987.
(42) Palmer, R. G.; Stein, D. L. In *Lectures in the Sciences of Complexity*; Stein, D. L., Ed.; Addison-Wesley: Redwood City, CA, 1989.
(43) Note that a rugged *free* energy surface can be obtained from a structureless *potential* energy surface through the introduction of dynamical constraints like forbidden pathways. The dynamical constraints introduce entropic barriers on the free energy surface. See ref 41.
(44) Fredrickson, G. H.; Andersen, H. C. *Phys. Rev. Lett.* **1984**, *53*, 1244; *J. Chem. Phys.* **1985**, *83*, 5822.
(45) Campbell, I. A.; Flesselles, J.-M.; Jullien, R.; Botet, R. *J. Phys. C* **1987**, *20*, L47; *Phys. Rev. B* **1988**, *37*, 3825.
(46) Fredrickson, G. H.; Brawer, S. A. *J. Chem. Phys.* **1986**, *84*, 3351.
(47) Press, W. H.; Flannery, B. P.; Teukolsky, S. A.; Vetterling, W. T. *Numerical Recipes*; Cambridge University Press: Cambridge, U.K., 1986.